# Correlated Energy-Spread Removal with Space Charge for High-Harmonic Generation

E. Hemsing, A. Marinelli, G. Marcus, and D. Xiang

Phys. Rev. Lett. **113**, 134802 — Published 22 September 2014

DOI: 10.1103/PhysRevLett.113.134802

# Correlated energy spread removal by space charge for high harmonic generation

E. Hemsing, A. Marinelli, and G. Marcus
*SLAC National Accelerator Laboratory, Menlo Park, California 94025, USA*

D. Xiang
*Key Laboratory for Laser Plasmas (Ministry of Education), Department of Physics and Astronomy, Shanghai Jiao Tong University, Shanghai 200240, China*

We study the effect of longitudinal space charge on the correlated energy spread of a relativistic high-brightness electron beam that has been density modulated for the emission of coherent, high harmonic radiation. We show that, in the case of electron bunching induced by a laser modulator followed by a dispersive chicane, longitudinal space charge forces can act to strongly reduce the induced energy modulation of the beam without a significant reduction in the harmonic bunching content. This effect may be optimized to enhance the output power and overall performance of free electron lasers that produce coherent light through high-gain harmonic generation. It also increases the harmonic number achievable in these devices, which are otherwise gain-limited by the induced energy modulation from the laser.

PACS numbers:

Free-electron lasers (FELs) use relativistic electron beams to produce widely tunable light with exceptional brightness at wavelengths down to hard x-rays for a broad range of studies [1]. At sub-optical wavelengths, FELs typically operate in self amplified spontaneous emission mode, or SASE [2–4], where the amplification process is initiated by noise in the electron beam. This shot noise is correlated only over extremely short timescales (typically a few femtoseconds for x-ray FELs), so for long electron beams the temporal and spectral SASE emission exhibits a large number of uncorrelated spikes and large statistical fluctuations.

To improve the FEL performance, high-gain harmonic generation (HGHG) is a technique used to stabilize the power output and to generate fully coherent radiation [5–7]. In HGHG, an external laser imprints a coherent modulation in the electron beam (e-beam) that then seeds FEL amplification of light at harmonics of the laser frequency. Because the modulation can be correlated over much longer timescales than SASE, the emitted light can have a much narrower bandwidth. In the standard HGHG setup, the laser first modulates the e-beam energy according to the transformation $\eta = \eta_0 + \delta\eta \sin(ks_0)$, where $\eta_0 = \Delta\gamma_0/\gamma \ll 1$ is the relative energy deviation of an electron within the e-beam with average energy $E = \gamma mc^2$, $s_0$ is the electron's longitudinal position within the beam, $\lambda = 2\pi/k$ is the laser wavelength, and $\delta\eta$ is the laser modulation amplitude. The e-beam then propagates through a dispersive section characterized by the transport matrix element $R_{56}$, which converts the energy modulation into a periodic density modulation according to $s = s_0 + R_{56}\eta$. Electrons are piled into sharp peaks longitudinally that are spaced at the laser wavelength, described by the distribution,

$$f_s(s) = 1 + 2\sum_{n=1}^{\infty} b_n \cos(nks), \tag{1}$$

where the density modulation is quantified by the e-beam bunching factor $b_n$. At a given harmonic $h$, the bunching factor for a beam with an initially uncorrelated Gaussian energy spread $\sigma_E$ is [5],

$$b_h = e^{-(hB)^2/2} J_h(-hAB), \tag{2}$$

where $A = \delta\eta/\sigma_{\eta_0}$ is the laser energy modulation amplitude relative to the relative energy spread $\sigma_{\eta_0} = \sigma_E/E$, $B = kR_{56}\sigma_{\eta_0}$ is the scaled dispersion, and $J_h$ is the Bessel function of order $h$.

The harmonic number in HGHG FELs is typically limited to $h \sim \rho/\sigma_{\eta_0}$ where $\rho$ is the FEL frequency bandwidth at saturation [8]. From Eq. (2) the optimal energy modulation to obtain significant bunching at the frequency $hkc$ is $A = 1/B \simeq h$. However, the FEL saturates when the e-beam energy spread approaches $\rho$, which is typically around $10\sigma_{\eta_0}$ in modern devices. Thus, the HGHG harmonic number is limited to approximately $h \lesssim 10 - 15$ to obtain high FEL output power with good temporal coherence [9].

Here, we propose and examine a scheme that enhances the power output from HGHG FELs, and can also boost the accessible harmonic number. Referred to as *quieted high gain harmonic generation*, or QHG, this technique exploits collective longitudinal space charge (LSC) effects generated by the sharp periodic density peaks to relinearize portions of the modulated e-beam phase space while preserving the harmonic bunching. The LSC effect takes place in a dedicated short drift or focusing section immediately downstream of the dispersive chicane which

may already exist as part of an HGHG FEL setup to help match the beam into the undulator (See Fig. 1). In this section, the phase space at the chicane exit (Fig 1a) is modified by the LSC forces produced by the density bunching. The result (Fig 1b) is a beam with sharp density spikes that coherently seed the HGHG process, but with a reduced projected energy spread between the spikes that facilitates lasing up to full saturation power. In principle, this approach may be used to increase the harmonic jumps in cascaded HGHG sections, or could replace 'fresh bunch' seeding techniques [10] in certain regimes to enable use of the whole beam to further reduce the saturated spectral bandwidth.

LSC effects in high-brightness beams have been examined recently in various different contexts, including the microbunching instability (see e.g., [11, 12]), LSC amplifiers [13, 14], shot noise suppression schemes [15–18], and as a method to generate a train of high peak-current bunches [19, 20]. Physically, LSC effects arise from the self-fields generated by longitudinal density perturbations in the beam. Electrons near each density peak, which have a width of $\Delta s \simeq \lambda/2A$ [21], receive an energy kick from the repulsive forces; those close in front of the peak experience a positive energy kick, while those close behind have their energy reduced (Fig 1c). In HGHG, the combination of the laser energy modulation and chicane dispersion used to generate harmonic bunching generates a nearly ideal initial longitudinal phase space distribution for the LSC forces to remove the positive energy chirp between density spikes. We refer to this portion as the working portion (WP) of the beam, (i.e, the region everywhere outside the $\sim 3\Delta s$ region at the spike), where the bulk of the harmonic FEL amplification process takes place. In e-beams with sufficiently small transverse and longitudinal emittances, the QHG effect works because the particle dynamics can be dominated by the motion in the energy space rather than in the longitudinal space.

We note that this HGHG enhancement scheme differs from other techniques that propose secondary phase-shifted laser modulations to partially reduce the energy spread [22–24]. QHG exploits the fact that the LSC forces are generated by the bunching structure and thus naturally phase-locked to the correlated energy modulation. This avoids precise timing constraints between successive laser modulation sections. Further, the shape of the harmonic LSC fields closely mirrors the phase space in the WP, allowing a nearly complete cancelation of the induced energy modulation in QHG (e.g., Fig 1d).

We describe the effect in a simplified model in which 3D effects can be neglected in the high-frequency limit where $\lambda$ is small compared to the transverse beam size $r_b$, namely, $\xi = kr_b/\gamma \gg 1$ [11, 25]. Transverse motion of particles is also neglected, assuming that the physical drift length is less than $\gamma\langle\beta\rangle/hk\epsilon_n$, where $\langle\beta\rangle$ is the average beta function and $\epsilon_n$ is the normalized emittance. In this regime, the general equations that describe evolution of the electron energy and longitudinal position in the e-beam frame are given as [19],

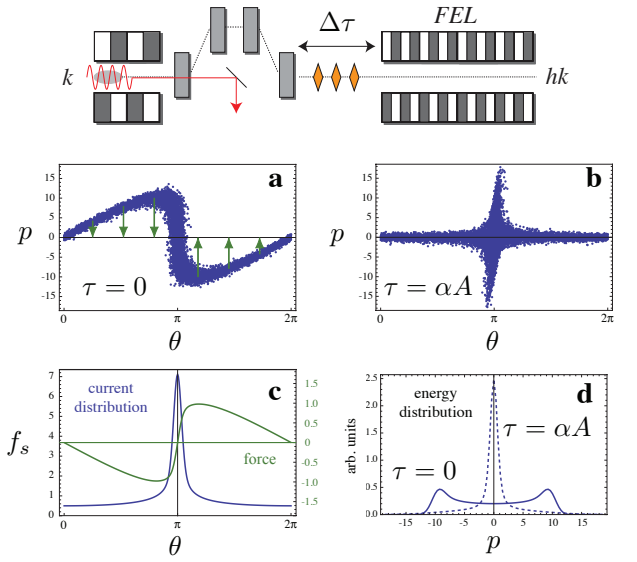


FIG. 1: Top: Layout of QHG scheme. (a) Phase space of the density modulated beam at the exit of the chicane (blue dots). The LSC fields give a kick to the nearby particles during a drift length $\tau$ (green arrows) that reverses the induced energy chirp, resulting in the distribution in (b). The initial sharp current spike shown in (c) produces the force distribution (green) that cancels the modulation and is essentially unchanged during the QHG drift. In (d), the projected energy distribution of the beam before the drift (solid line) shows the characteristic double horn shape, but returns to a narrow spike with a significantly reduced energy spread afterward (dashed line).

$$\begin{aligned} \frac{d\eta}{dz} &= \frac{q}{\gamma mc^2} E_z \\ \frac{ds}{dz} &= \frac{\eta}{\gamma^2} \\ \frac{dE_z}{ds} &= \frac{qn_0}{\epsilon_0} f_s(s) \end{aligned} \tag{3}$$

where $-q$ is the charge of an electron, $n_0$ is the beam volume density and $E_z$ is the longitudinal space charge field. Inserting the longitudinal distribution of the bunched beam from Eq. (1), the space-charge fields due to the periodic bunching structure are,

$$E_z = \frac{2qn_0}{\epsilon_0 k} \sum_{n=1}^{\infty} b_n \frac{\sin(nks)}{n}. \tag{4}$$

It is convenient to rescale the variables and define $p = \eta/\sigma_{\eta_0}$ as the scaled energy, $\tau = k_p z$ as the plasma phase advance starting from the chicane exit, $k_p^2 = q^2 n_0/m\epsilon_0 c^2\gamma^3$, and $\theta = ks$ as the phase position of a particle in the beam with respect to the laser. From the

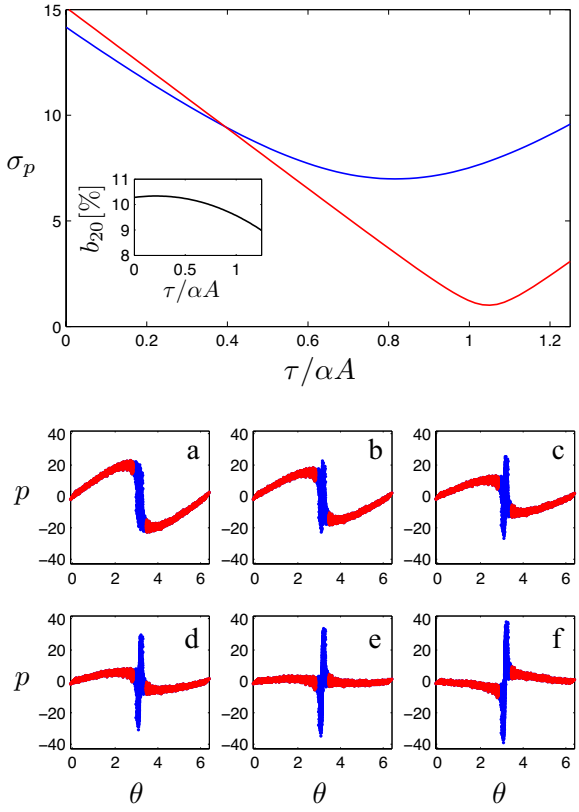


FIG. 2: Top: Evolution of the relative energy spread for the whole beam (blue) and the WP just outside the density spike (red). Inset: Evolution of the bunching factor for the 20th harmonic. Bottom: Phase space evolution along the drift.

LSC fields in Eq. (4), we obtain two non-linear equations that describe the evolution:

$$\begin{aligned} \frac{dp}{d\tau} &= \frac{2}{\alpha}\sum_{n=1}^{\infty} b_n \frac{\sin n\theta}{n}, \\ \frac{d\theta}{d\tau} &= \alpha p. \end{aligned} \tag{5}$$

Note that $b_n = b_n(\tau)$. We have also defined

$$\alpha = \frac{k\sigma_{\eta_0}}{k_p\gamma^2}, \tag{6}$$

which is the energy spread parameter and sets the scale for the overall dynamics. It can be interpreted as the ratio of the longitudinal displacement due to thermal motion in a plasma period to the laser wavelength. The QHG regime requires $\alpha \ll 1$ and the thermal motion can be neglected on the time scale of the plasma period [25].

The QHG scaling is obtained by linearizing the dynamical equations for small changes in the phase space position of a particle during the drift. Namely, we assume $\theta(\tau) \simeq \theta(0) + \Delta\theta(\tau)$, where $\Delta\theta(\tau) \ll 1$, and $\theta(0)$ is the initial position at $\tau = 0$. Similarly, the change in energy is $p(\tau) \simeq p(0) + \Delta p(\tau)$ where $\Delta p < p(0)$. The scaling of a beam optimized for density bunching at the harmonic $h = A \gg 1$ is dominated by the $n = 1$ space-charge term in Eq. (5). Accordingly, in this linear model, particles near the position $(p(0), \theta(0)) = (A, \pi/2)$ experience the largest changes in energy and phase position. The optimal bunching factor $b_1 \simeq -AB/2 = -1/2$ is constant in the $\Delta\theta(\tau) \ll 1$ limit, so both equations can be integrated directly over a short drift $\Delta\tau$ to give $\Delta p \simeq -\Delta\tau/\alpha$ and $\Delta\theta \simeq \alpha A\Delta\tau$. The drift length over which the initial energy modulation induced by the laser $\Delta p \simeq A$ is approximately canceled by space charge effects is then

$$\Delta\tau \simeq \alpha h. \tag{7}$$

The corresponding change in phase is approximately $\Delta\theta \simeq \alpha h\Delta\tau \simeq (\alpha h)^2$.

The natural dispersion of particles with different energies requires that,

$$\Delta\theta < 1/h, \tag{8}$$

such that the change in position is less than the desired harmonic wavelength $\lambda_h = 2\pi/k_h = \lambda/h$ in order to preserve bunching at $h$. The approximate limit on the scaled drift length is then $\Delta\tau < \sqrt{1/h}$. Together, Eqs. (7) and (8) constrain the parameter $\alpha$ to,

$$\alpha < \sqrt{1/h^3}. \tag{9}$$

If satisfied, Eq (9) states that the bunching factor at the harmonic $h$ remains essentially unchanged during the drift $\Delta\tau \simeq \alpha h$, and that the correlated energy spread in the WP induced by the laser is approximately minimized.

An example of the QHG process is shown Fig 2, where we follow the evolution of the scaled energy spread $\sigma_p = \sqrt{\langle p^2\rangle}$ and corresponding phase space of a beam along a drift. Results are obtained from particle simulations governed by the 1D equations in Eqs. 5. We take $\alpha = 0.005$, and the beam starts with an initial modulation of $A = 20 = 1/B$ (Fig. 2a) that optimizes bunching at $h = 20$. The beam is shown by the blue particles, some of which are obscured by the overlaid red particles that identify only particles in the WP. During the drift the energy modulation is steadily reduced by the LSC forces (Figs 2b through e). The relative rms energy spread of all of the particles (blue line, upper plot) reaches a minimum near $\tau \simeq 0.8\alpha A$, (see Fig 2d). However, considering only the particles in the WP, the energy spread continues to decrease (red line, upper plot) and is minimized at $\tau \simeq \alpha A$ (Fig 2e) where the distribution of the red particles appears flat with an energy spread almost exactly equal to the initial value ($\sigma_p = 1$). This is the end of the QHG process, at which point the transverse size is expanded to arrest the LSC effects. Otherwise the beam overshoots the minimum in energy spread (Fig. 2f). Along the drift, the bunching factor at the

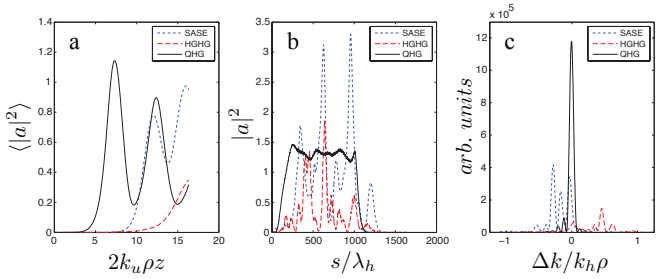


FIG. 3: FEL output power (a), temporal profile (b), and spectrum (c) for SASE, HGHG, and QHG scenarios.

20th harmonic (Fig 2 top, inset) decreases slightly due primarily to longitudinal dispersion, but remains significantly larger than the shot noise such that the coherent harmonic signal dominates in the FEL.

To evaluate the performance of the QHG beam in an FEL, we performed time-dependent 1D FEL simulations for a simple case. Results are shown in Fig. 3 and are compared with HGHG and SASE. The beam is assumed to have a flat initial current profile (before modulation) and lases in an FEL tuned to the 20th harmonic of the laser modulation, which covers the entire beam. The simulation code is a variant of standard 1D FEL codes and calculates the performance using the high-gain FEL evolution equations based on the exact input particles. However, it also allows for each of the slices that define the resonant FEL wavelength $\lambda_h$ to have a different number of electrons, as would be the case in the physical density modulated beam. The simulations also permit electrons to pass between different slices each undulator period to account for the effects of dispersion inside the FEL. This feature is needed to accurately model the modulated beams in QHG and HGHG where particles have large energy deviations and shift significantly in phase. The dynamics are calculated in general form for an FEL specified by $\rho$ according to the commonly scaled variables for relative energy $\eta/\rho$, phase $\theta_h = k_h s$, complex field amplitude $a$, and longitudinal coordinate $2k_u\rho z$, where $\lambda_u = 2\pi/k_u$ is the undulator period [26].

In this example we take $\rho = 2\times10^{-3}$ and $\sigma_{\eta_0} = \rho/10$, similar to parameters in modern soft x-ray FELs. In Fig. 3a the radiation power along the undulator is shown for each scenario. The unmodulated SASE beam (blue line) reaches saturation ($\langle|a|^2\rangle \simeq 1$) after $\sim$20 gain lengths $L_g = 1/2\sqrt{3}k_u\rho$ as expected from high-gain FEL theory. The HGHG beam fully saturates at a reduced power level (red line) and has a longer gain length due to the uncompenstated energy structure from the laser. The QHG beam reaches full saturation power (black line) at the halfway mark thanks to the removed energy chirp in the WP. The effect of reducing the energy modulation in QHG is also evident in the temporal and spectral structure of the output radiation (Figs. 3b and c). The pulse from QHG has a roughly flat temporal profile at saturation and a narrowband spectrum with rms bandwidth $\Delta k/k_h = 0.03\rho$. This is compared with the SASE and HGHG cases at their respective saturation levels which both exhibit multiple temporal and spectral spikes and have a full bandwidth of $\sim\rho$. The premodulated beam in the HGHG case thus only reduces the output power without reducing the bandwidth. In the QHG case, however, the output pulse is temporally coherent and the bandwidth is determined simply by the beam length, which is $1000\lambda_h$ or approximately five coherence lengths $l_c \simeq \lambda_h/\sqrt{2\pi}\rho$. This is consistent with the number of temporal spikes seen in the SASE case. The narrow QHG spectrum results because the cooperation length $L_c = \lambda_h L_g/\lambda_u \simeq 23\lambda_h$ is slightly longer than the distance between density spikes. This enables phase information in the amplified radiation to be communicated between density spikes over each gain length, which flattens out the temporal profile and narrows the spectrum. Narrowing the spectrum further is just a matter of using longer e-beams.

The differences between the QHG and HGHG beams are illustrated by inspection of the phase space evolution during FEL amplification. Shown in Fig. 4a, the HGHG beam retains a large energy correlation in the WP. As amplification of the 20th harmonic signal develops, only a portion of the particles near the center of the WP fully participate in the interaction. Particles with the largest energy deviation are outside the seeded FEL bandwidth and are thus detuned in frequency. Further, dispersion acts to slowly decompress the local chirp and shift the developing energy modulation to longer wavelengths. This competes with the resonant FEL wavelength, and beat waves in the energy modulation emerge. The resulting frequency competition appears to suppress gain and leads to a multi-spike spectral structure. Conversely, the QHG beam in Fig. 4b has a flattened WP that permits monochromatic amplification. The particles in the WP

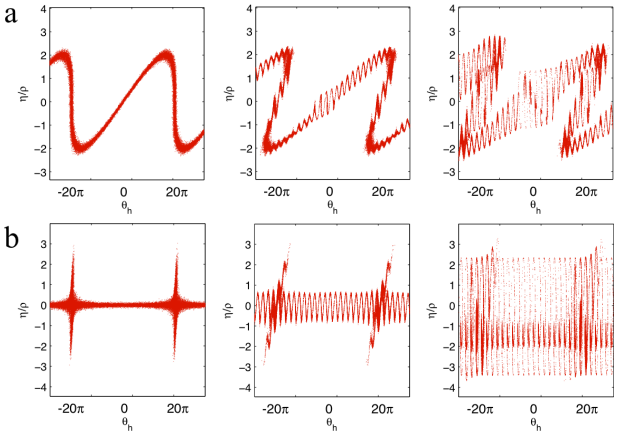


FIG. 4: Evolution of the e-beam phase space in a) HGHG and b) QHG during amplification of the 20th laser harmonic.

contribute uniformly to the FEL instability which generates more output power. Dispersion also acts in this case to tilt the phase space of the particles with the large residual energy deviation at each spike. This leads to an observable dip in the harmonic bunching factor early on (not shown), but at that point the coherent amplification process has been sufficiently developed that the FEL output is essentially unaffected.

We note that e-beams characterized by non-Gaussian energy spreads have been predicted to permit FEL saturation at $h > 15$ in HGHG [9]. The impact of the QHG scheme on such beams is worthy of additional investigation, as this approach could further improve the harmonic range and FEL performance through similar reductions in the WP energy spread.

Finally, 3D effects are likely to play an important role in the implementation of this scheme in practice, particularly for beams where $\xi = r_b k/\gamma \lesssim 1$ because the harmonic $E_z$ fields are each reduced and reshaped by a factor $F_n(r,\xi) \leq 1$ which depends on the transverse distribution [11, 25]. For a flat top distribution of radius $r_b$, for example, this factor is $F_n(r,\xi) = 1 - n\xi I_0(n\xi r/r_b)K_1(n\xi)$, and 3D effects can be included by inserting $F_n$ into the sum in Eq. (5). The drift length in (7) is then increased to $\Delta\tau \simeq \alpha h/F_1(0,\xi)$, and the energy spread parameter constraint is $\alpha < \sqrt{F_1(0,\xi)/h^3}$. For a flat top beam $\alpha$ can be written in practical units as $\alpha = \xi\sigma_{\eta_0}\sqrt{\gamma I_A/4I_0}$, where $I_A = 17$ kA and $I_0$ is the peak current in the beam. From this scaling, a 1 GeV beam with $I_0 = 5$ kA and $\sigma_{\eta_0} = 10^{-4}$, for example, requires a $\Delta\tau/k_p = 2.7$ m drift at a spot size of $r_b = 150$ $\mu$m to reduce the WP energy spread by a factor of 4 for the 20th harmonic of a 240 nm laser modulation ($\xi = 2$, $\alpha = 0.008$). In general, these effects depend sensitively on the beam parameters and are the subject of future studies.

The authors thank Y. Ding for useful discussions. This work was supported by the U.S. Department of Energy under Contract No. DE-AC02-76SF00515.

[1] B. W. J. McNeil and N. R. Thompson, Nat. Photonics **4**, 814 (2010).
[2] P. Emma, *et al.*, Nature Photonics **4**, 641 (2010).
[3] T. Ishikawa, H. Aoyagi, T. Asaka, Y. Asano, N. Azumi, T. Bizen, H. Ego, K. Fukami, T. Fukui, Y. Furukawa, et al., Nat. Photonics **6**, 540 (2012).
[4] W. Ackermann, G. Asova, V. Ayvazyan, A. Azima, N. Baboi, J. Bahr, V. Balandin, B. Beutner, A. Brandt, A. Bolzmann, et al., Nat. Photonics **1**, 336 (2007).
[5] L. H. Yu, Phys. Rev. A **44**, 5178 (1991).
[6] L.-H. Yu, M. Babzien, I. Ben-Zvi, L. F. DiMauro, A. Doyuran, W. Graves, E. Johnson, S. Krinsky, R. Malone, I. Pogorelsky, et al., Science **289**, 932 (2000).
[7] E. Allaria, R. Appio, L. Badano, W. Barletta, S. Bassanese, S. Biedron, A. Borga, E. Busetto, D. Castronovo, P. Cinquegrana, et al., Nature Photon. **6**, 699 (2012).
[8] R. Bonifacio, C. Pellegrini, and L. M. Narducci, Optics Communications **50**, 373 (1984).
[9] E. Ferrari, E. Allaria, W. Fawley, L. Giannessi, Z. Huang, G. Penco, and S. Spampinati, Phys. Rev. Lett. **112**, 114802 (2014).
[10] E. Allaria, D. Castronovo, P. Cinquegrana, P. Craievich, M. Dal Forno, M. Danailov, G. D'Auria, A. Demidovich, G. De Ninno, S. Di Mitri, et al., Nature Photon. **7**, 913 (2013).
[11] M. Venturini, Phys. Rev. ST Accel. Beams **11**, 034401 (2008).
[12] A. Marinelli and J. B. Rosenzweig, Phys. Rev. ST Accel. Beams **13**, 110703 (2010).
[13] E. A. Schneidmiller and M. V. Yurkov, Phys. Rev. ST Accel. Beams **13**, 110701 (2010).
[14] A. Marinelli, E. Hemsing, M. Dunning, D. Xiang, S. Weathersby, F. O'Shea, I. Gadjev, C. Hast, and J. B. Rosenzweig, Phys. Rev. Lett. **110**, 264802 (2013).
[15] A. Gover and E. Dyunin, Phys. Rev. Lett. **102**, 154801 (2009).
[16] D. Ratner, Z. Huang, and G. Stupakov, Phys. Rev. ST Accel. Beams **14**, 060710 (2011).
[17] D. Ratner and G. Stupakov, Phys. Rev. Lett. **109**, 034801 (2012).
[18] A. Gover, A. Nause, E. Dyunin, and M. Fedurin, Nature Physics **8**, 877 (2012).
[19] P. Musumeci, R. K. Li, and A. Marinelli, Phys. Rev. Lett. **106**, 184801 (2011).
[20] P. Musumeci, R. K. Li, K. G. Roberts, and E. Chiadroni, Phys. Rev. ST Accel. Beams **16**, 100701 (2013).
[21] A. A. Zholents, Phys. Rev. ST Accel. Beams **8**, 040701 (2005).
[22] B. W. J. McNeil, G. R. M. Robb, and M. W. Poole, in *Proceedings of the 2005 Particle Accelerator Conference, Knoxville, Tennessee* (2005).
[23] E. Allaria and G. De Ninno, Phys. Rev. Lett. **99**, 014801 (2007).
[24] Q. Jia, Applied Physics Letters **93**, 141102 (2008).
[25] A. Marinelli, E. Hemsing, and J. B. Rosenzweig, Physics of Plasmas **18**, 103105 (2011).
[26] Z. Huang and K.-J. Kim, Phys. Rev. ST Accel. Beams **10**, 034801 (2007).